J. Fluid Mech. (1998), *vol.* 370, *pp.* 73–99 Printed in the United Kingdom

Experiments on vortex breakdown in a confined flow generated by a rotating disc

By A. SPOHN[1], M. MORY[2] AND E. J. HOPFINGER[2]

[1] Laboratoire d'Etudes Aérodynamiques; ENSMA UMR-CNRS 6609, BP 109, 86960 Futuroscope Cedex, France

[2] Laboratoire des Ecoulements Géophysiques et Industriels, UJF-CNRS, BP 53X, 38041 Grenoble Cedex, France

(Received 17 July 1995 and in revised form 17 April 1998)

The steady-state flow generated by a rotating bottom in a closed cylindrical container and the resulting vortex breakdown bubbles have been studied experimentally. By comparing the flow inside two different container geometries, one with a rigid cover and the other with a free surface, we examined the way in which the formation and structure of the breakdown bubbles depend on the surrounding flow. Details of the flow were visualized by means of the electrolytic precipitation technique, whereas a particle tracking technique was used to characterize the whole flow field. We found that the breakdown bubbles inside the container flow are in many ways similar to those in vortex tubes. First, the bubbles are open with in- and outflow and second, their structure is, like in the case of vortex breakdown in pipe flows, highly axisymmetric on the upstream side of the bubble and asymmetric on their rear side. However, and surprisingly, we observed bubbles which are open and stationary at the same time. This shows that open breakdown bubbles are not necessarily the result of periodic oscillations of the recirculation zone. The asymmetry of the flow structure is found to be related to the existence of asymmetric flow separations on the container wall. If the angular velocity of the rotating bottom is increased the evolution of the breakdown bubbles is different in both configurations: in the rigid cover case the breakdown bubbles disappear but persist in the free surface case.

1. Introduction

Under certain conditions vortex flows undergo sudden structural changes near their rotation axis, called vortex breakdown, which are characterized by the existence of a free stagnation point upstream of a region with reversed axial flow. Although more than 40 years have passed since the first investigation of this phenomenon by Peckham & Atkinson 1957 (see Escudier 1988), even basic features of vortex breakdown such as flow symmetry, steadiness and internal flow structure are still subject to considerable controversy (Escudier 1988; Granger 1990). The three-dimensional and highly responsive character of vortex flows do not yet allow phenomena inherent to vortex breakdown and other concomitant phenomena to be clearly distinguished. This is also one of the reasons why it is so difficult to determine the relevant physical mechanisms leading to vortex breakdown. Several theories based on very different physical concepts as hydrodynamic instability, finite supercritical–subcritical transition, wave propagation and similarity with boundary layer separation have been proposed. For detailed descriptions of these theories the reader is referred to the reviews by Hall (1967, 1972), Leibovich (1978, 1984) and Escudier (1988). More needs to be known about the

characteristics of the breakdown phenomenon itself in order to be able to carry out conclusive tests of the different theories.

Numerous studies of vortex breakdown were carried out in vortex tubes where the swirl was generated by inlet guidevanes (Harvey 1962; Sarpkaya 1971; Faler & Leibovich 1977, 1978 and others) or similar arrangements, as for example in tubes with an axial slit for tangential inflow (see Escudier 1988). Vogel (1968, 1975) and Escudier (1984) showed the existence of recirculation bubbles of vortex breakdown type in the flow generated by a rotating endwall of a closed cylindrical container. According to the experiments of Vogel (1968) and Escudier (1984) the formation of these recirculation bubbles depends on the container aspect ratio H/R, H and R being respectively the height and the inner radius of the cylinder, and on the Reynolds number $Re = \Omega R^2/\nu$, where Ω is the angular velocity of the rotating bottom and ν the kinematic viscosity. Escudier (1984) determined the parameter domain (H/R, Re) for which one, two or even three breakdown bubbles can be observed. Spohn, Mory & Hopfinger (1993) extended this type of study to container flow with a free surface in which case the occurrence of recirculation bubbles and their position are different (that is the bubbles can be attached to the free surface).

The absence of in- and outflow boundaries and the axisymmetric container geometry is advantageous for numerical simulations of the boundary conditions. Axisymmetric numerical simulations were conducted by Lugt & Haussling (1982), Lugt & Abboud (1987), Neitzel (1988), and Lopez (1990). In all cases the calculated position and number of the breakdown bubbles was found to be in good agreement with the flow visualizations of Escudier (1984). Lopez & Perry (1992) also used axisymmetric numerical simulations to analyse more closely the structure of the breakdown bubbles. Their calculations seem to indicate that for steady flow the streamlines inside the breakdown bubbles are closed and bubbles with in- and outflow are restricted to unsteady flow regimes. This is of particular interest since most observations of breakdown bubbles made in vortex tubes highlight the asymmetric and open character of the bubble (Brücker & Althaus 1992; Leibovich 1978 among others). Moreover, based on their numerical simulations of vortex breakdown in open systems with throughflow, Krause & Liu (1989) and Spall, Gatski & Ash (1990) among others, claimed that vortex breakdown can only be understood as an unsteady, asymmetric three-dimensional phenomenon. Recent comparisons between axisymmetric and non-axisymmetric simulations of the breakdown bubble made by Menne & Liu (1990) confirm this point of view. These observations highlight that the recirculation bubbles inside the container flow show some particular characteristics which deserve further investigation in order to clarify differences and similarities with previous observations of vortex breakdown.

Most of the previous container flow experiments used either the fluorescent dye technique with on-axis injection of dye to visualize the position and number of breakdown bubbles (Vogel 1975; Escudier 1984; Böhme, Rubart & Stenger 1992; Spohn *et al.* 1993) or focused on the global velocity field (Ronnenberg 1977, Vogel 1968). Neither technique allowed the analysis of the inner structure of the breakdown bubbles as precisely as was done numerically by Lopez (1990). The present experiments aim to fill this gap and focus on what seems to us an important aspect, namely the way in which the position and structure of the breakdown bubbles are related to the global structure of the container flow around the breakdown bubbles. For this purpose we also compared flow and breakdown conditions with a rigid cover and with a free surface. The flow structure has been visualized with the help of the electrolytic precipitation technique. In contrast to dye techniques this method ensures a uniform

release of the tracer directly on the container walls outside the axis of symmetry so that flow separations which characterize the flow structure can be captured. In order to analyse the velocity field around the breakdown bubbles quantitatively we measured the velocity field by a particle tracking technique.

The present study reveals some interesting new details of the container flow. Among these are asymmetric separations on the cylinder wall and the existence of non-axisymmetric, stationary breakdown bubbles with in- and outflow. We note also the close connection between the disappearance of the breakdown bubbles at higher Reynolds numbers and the increasingly cylindrical character of the central vortex flow. In §2 we describe the experimental arrangement. The results of flow visualizations and velocity measurements are presented in §3. In §4 we discuss our observations in the context of previous studies of the container flow and the vortex breakdown phenomenon. In particular we highlight some new aspects of the bubble structure inside the container flow which further illustrate their similarity with breakdown bubbles in open systems.

2. Experimental arrangement

2.1. *Apparatus*

The visualization experiments were carried out in a cylindrical container made of clear Perspex with 91.3 mm inner diameter (figure 1). The upper boundary was either a rigid cover or a free surface. The height of the flow domain H could be varied by changing the position of the cover, or by changing the fluid depth inside the container. The rotating bottom was driven by an electric motor drive with the rotation speed Ω controlled continuously by a microprocessor. During the experiments the variations of Ω were less than 0.2 %. The gap between the rotating bottom and the cylinder wall and also between the rigid cover and the cylinder was about 0.3 mm. The whole cylindrical container was placed inside a rectangular box of dimensions $460 \times 460 \times 600$ mm filled with water up to a height of 450 mm. By recirculating this water permanently through a constant temperature bath, it was possible to keep the temperature of the working fluid constant within ± 0.2 °C. In all experiments reported here, the measured temperature gradient between the air above the free surface and the fluid in the test section was less than 0.5 °C. The velocity measurements were carried out in a second installation with a larger container of 110 mm inner diameter.

Most of the experiments were carried out with tap water as working fluid. In some experiments a glycerine–water mixture was also used. The Reynolds number $Re = \Omega R^2/\nu$ could be varied in the range $1000 \leqslant Re \leqslant 40000$ and the aspect ratio H/R in the range $0.5 \leqslant H/R \leqslant 4$. However, in this paper we focus on results obtained for Re in the interval [1000, 6000] and H/R within [1, 2.0]. The relation $(H/R)\,Gr/Re^2 = g\alpha\Delta T H^3/\nu^2 \times 1/Re^2$, where Gr is the Grashof number, g the acceleration due to gravity, α the coefficient of thermal expansion and ΔT the temperature difference, compares the importance of the thermal convection produced by temperature perturbations to the forced convection driven by the rotating disc. In all experiments it remained smaller than 0.13. In the free surface case the Froude number $Fr = \Omega^2 R^2/Hg$ varied in the range [0.002, 0.017]. The maximal relative depression h/H of the interface, which was caused by the rotation of the fluid, did not exceed 0.02.

2.2. *Measurement techniques*

The electrolytic precipitation, described by Honji, Taneda & Tatsuno (1980), was adapted to the container flow. As indicated in figure 1 the flow was marked at two

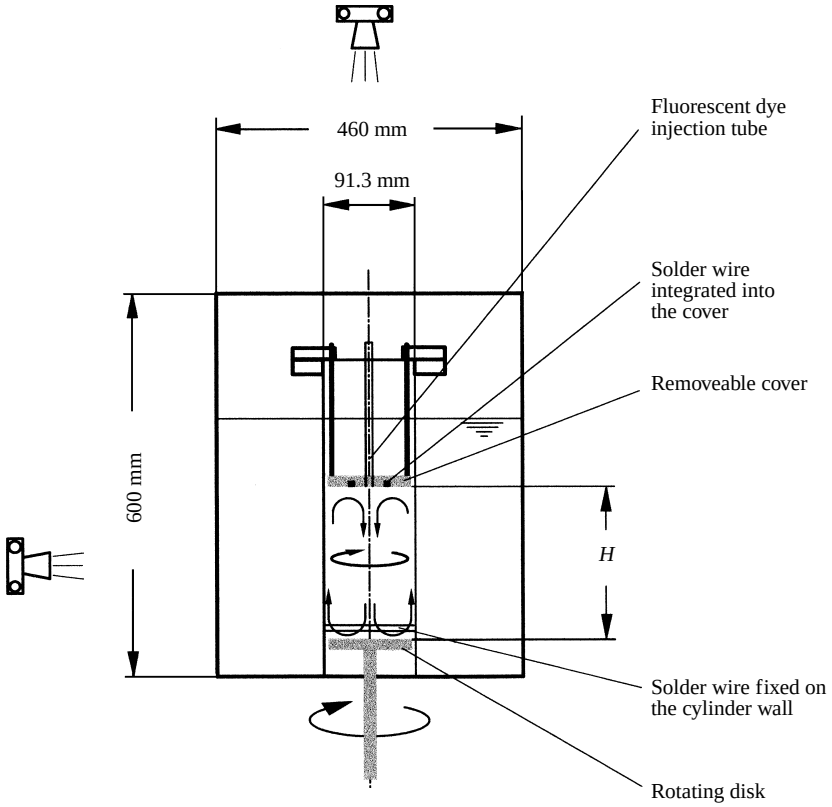

FIGURE 1. Schematic of the experimental set-up showing the two positions of the solder wires used for electrolytic precipitation. One solder wire is integrated into the removable transparent cover, the other one is fixed on the cylinder wall at about 4 mm above the rotating disc. The flow can be observed in horizontal planes perpendicular to the container axis or in vertical planes across the flow domain.

different positions. To observe the flow near the walls and around the breakdown bubbles a flat solder wire of 0.08 mm thickness was fixed at the inner perimeter of the cylinder wall at about 4 mm above the rotating disc. When applying a constant potential of 1.5 V the wire released uniformly a white powder which was carried along with the flow. The inner structure of the recirculation bubbles could be better analysed by releasing the tracer from the rigid cover. For this purpose a second wire was positioned in the cover in a 1 mm $\times$ 1 mm circular groove of 30 mm diameter. The solder wire was pressed into this groove so that it was flush with the surface of the cover. With this wire the best results were obtained by applying rectangular voltage pulses of about 15 V with a frequency of about 10 Hz. To visualize the flow structure in cross-sections we used in both cases the light scattered by the released powder during its motion inside a sheet of light, like in the case of the fluorescent dye technique, previously used by Vogel (1975) among others. The sheet of light of 1 mm thickness was produced by expanding the light beam of a 5 W Argon laser with a cylindrical lens. The intensity of the light beam did not exceed 2 W. To get different views of the flow structure the sheet could be directed in three different planes. Most of the visualizations were carried out in a vertical diametral plane giving access to the secondary flow. The evolution of the azimuthal flow was examined in several horizontal cross-sections at different distances from the rotating disc. Finally, for some particular experiments the

light sheet was enlarged to 10 mm thickness and oriented in a plane tangential to the inner side of the cylinder wall to study the distribution of the shear stress direction on this wall. In all cases the observed tracer distribution was recorded by a Sony video camera. Due to the outer rectangular water bath the distortion of the diametral plane on the video pictures was reduced to values less than 4 % with the exception of a 5 mm bright band along the cylinder wall. The time of each video frame was measured relative to the start-up time of the rotating disc. Complementary visualizations were also performed by the fluorescent dye technique as was used by Escudier (1984). In this case the dye was injected through a tube with 0.3 mm inner diameter in the centre of the cover plate.

The velocity field was measured by particle velocimetry. Neutrally buoyant polystyrene beads of about 0.4 mm diameter were added to the fluid and used as tracer particles. The light scattered from these particles during their motion inside a sheet of light was recorded by a Nikon F2 camera on a JP4 black and white film (125 ASA). Although, in strictly two-dimensional flow such photographs would be sufficient to determine the magnitude of the velocity vectors, several difficulties arise in the case of the three-dimensional container flow. First, since the tracer particles are continuously recirculated along their three-dimensional trajectories some of them always enter or leave the sheet of light during the exposure time and cause misrepresentations. This error is particularly important in measurements of the axial and radial velocities in a vertical diametral plane. This is because the larger azimuthal velocities are directed perpendicular to the measurement plane. Second, the velocity vectors of the secondary flow change their direction inside different regions of the flow domain and, thus, make it also necessary to detect their direction. To overcome both of these difficulties we refined our technique. The thickness of the light sheet was enlarged to 8 mm to permit longer exposure times and the total exposure time of the camera was divided into a sequence of one short and two long intervals by means of a programmable mechanical shutter, which was mounted in front of the camera. During the following analysis of the photographs the known time interval between the end of the first short exposure time and the beginning of the second long exposure time allowed the magnitude and direction of the velocity vectors inside the measurement plane to be determined, whereas incomplete streak sequences could be eliminated from processing. The position and length of valid particle paths were measured with the help of a manual digitalization table (Benson 6021) on which we projected the negative of the photographs. Finally, these numerical data were used to determine the velocity vectors.

2.3. *Validation of the installation*

To test the validity of our experimental installation and also to confirm the possibility of using water as working fluid we carried out some preliminary visualizations. In the first two experiments we chose the rigid cover configuration to compare, for some selected parameters (H/R, Re), the number and position of breakdown bubbles with previous observations of Escudier (1984). First, we used, like Escudier, glycerine–water mixtures (60 % glycerine) in combination with the fluorescent dye technique. Second, we used tap water as working fluid and the electrolytic precipitation technique. In both cases the visualizations were in good agreement with Escudier's findings. Figure 2 shows the result of the second case. Neither the reduction of the container diameter (i.e. Escudier used a cylinder with $R = 100$ mm), nor the use of water as working fluid led to visible differences, indicating that H/R and Re are the relevant scaling parameters.

Furthermore, we compared for some selected parameter combinations (H/R, Re) the results obtained in the free surface case with our previous observations (Spohn *et*

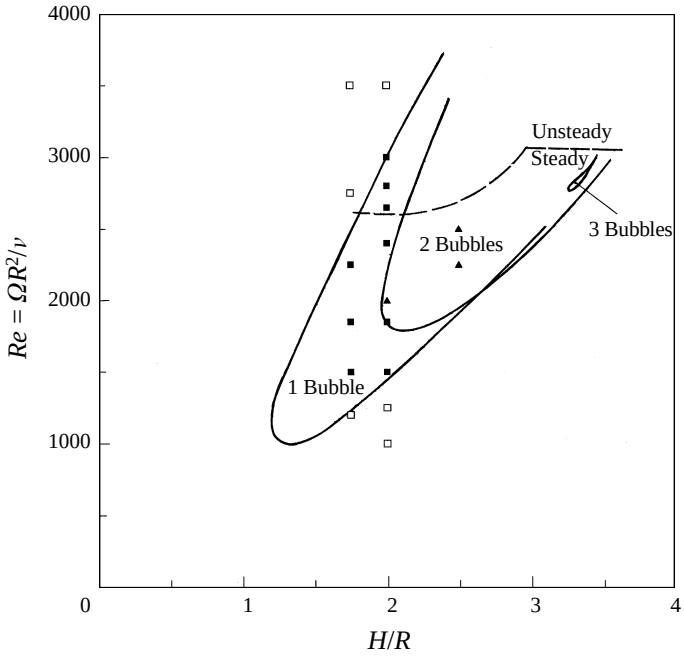

FIGURE 2. Comparison of flow states with a rigid cover for some selected parameter combinations (H/R, Re) with the results obtained by Escudier (1984). The working fluid is water and the electrolytic precipitation technique was used. Regimes where experiments have been carried out are indicated by symbols: □, no bubble; ■, one bubble; ▲, two bubbles.

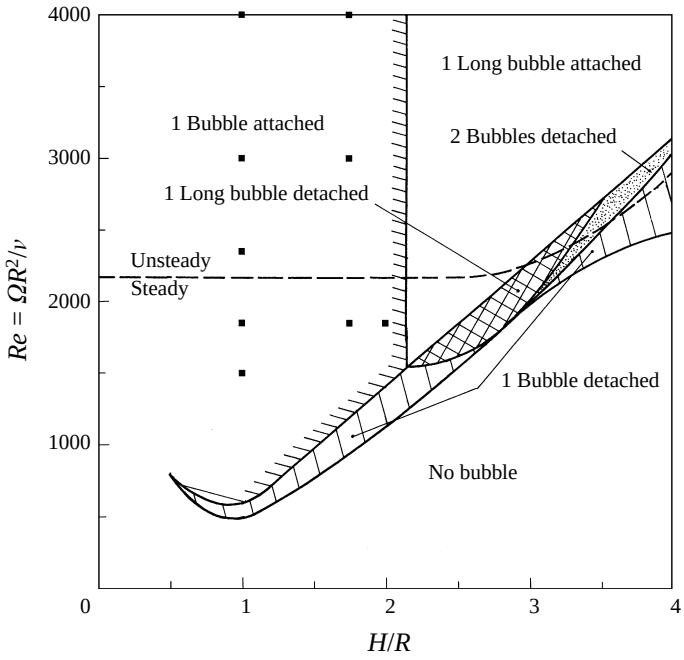

FIGURE 3. Comparison of flow states with a free surface for some selected parameter combinations (H/R, Re) with the results obtained by Spohn *et al.* (1993). The working fluid is water and the electrolytic precipitation technique was used. Regimes where experiments have been carried out are indicated by symbols: ■, one bubble.

al. 1993). Instead of glycerine–water mixtures and the fluorescent dye technique we used again tap water as working fluid and visualized the flow with the electrolytic precipitation technique. Figure 3 shows that the results are also in good agreement with our previous observations. However, we observed that the use of water made the flow for $H/R > 3$ and $Re < 1500$ more sensitive to perturbations. In particular, occasional shocks off the laboratory floor led to dramatic changes of the flow structure. To avoid these difficulties all experiments with a free surface presented here were made for $H/R < 3$ and $Re \geqslant 1500$.

The boundary conditions at the free surface strongly depend on the chemical composition of the interface. Clean surfaces without contamination by surface-active molecules are hard to realize experimentally (see Davis & Rideal 1963). In the present study we were not able to control the chemical composition of the surface. Thus, the formation of surface films with special mechanical properties, different from those in the bulk, could not be excluded. However, all flow structures presented here were reproducible and did not depend on the working fluid or the visualization technique. This suggests that possible changes of the composition of the free surface did not cause any observable modifications of the flow structure. During all experiments small floating dust particles showed an azimuthal velocity indicating that the azimuthal stresses were negligible or small.

3. Results

3.1. *Deviations from symmetry*

Careful visualizations of the flow structure show asymmetric aspects at all Reynolds numbers although the container geometry is nearly perfectly axisymmetric. To fix ideas we illustrate such asymmetric aspects in the rigid cover case for $H/R = 1.75$ and $Re = 1850$. In figure 4(*a*) the flow structure is visualized by the fluorescent dye technique, whereas figure 4(*b*,*c*) shows the same flow visualized by the electrolytic precipitation method. In all three cases the working fluid was tap water. The fluorescein dye was added to the flow from a tube of 0.3 mm inner diameter placed at the centre of the cover. The powder produced by electrolytic precipitation was either released from the solder wire at the rigid cover (figure 4*b*) or from the solder wire mounted on the cylinder wall (figure 4*c*). All three methods revealed stationary flow with one breakdown bubble in agreement with Escudier (1984). However, although we used in all three cases an axisymmetric emission of tracer particles, we can see in all figures an asymmetric distribution of the tracer particles. The particular manifestations of this asymmetry depend on the visualization technique employed. However, all show the same asymmetry. A comparison of figures 4(*b*) and 4(*c*) shows this particularly clearly since each image indicates on the downstream side of the bubble the inverted image of the other, much like a photograph and its negative. This demonstrates that the observed asymmetry is not caused by symmetry defaults of the visualization techniques employed. This is further confirmed by visualizations of the powder distribution taken shortly after the electrolytic precipitation was started. Figure 5(*a*,*b*) shows two examples of such visualizations for the case with electrolytic precipitation at the rigid cover. Neither in the horizontal plane adjacent to the cover, nor in a vertical diametral plane can we see any asymmetries. Clearly the electrolytic precipitation supplied tracer particles in a highly axisymmetric way. Finally, it should be pointed out that the asymmetry of the recirculation bubbles, visible in figure 4, is not always so obvious and depends on the flow parameters (H/R, Re). Figure 6 illustrates, for example, the more

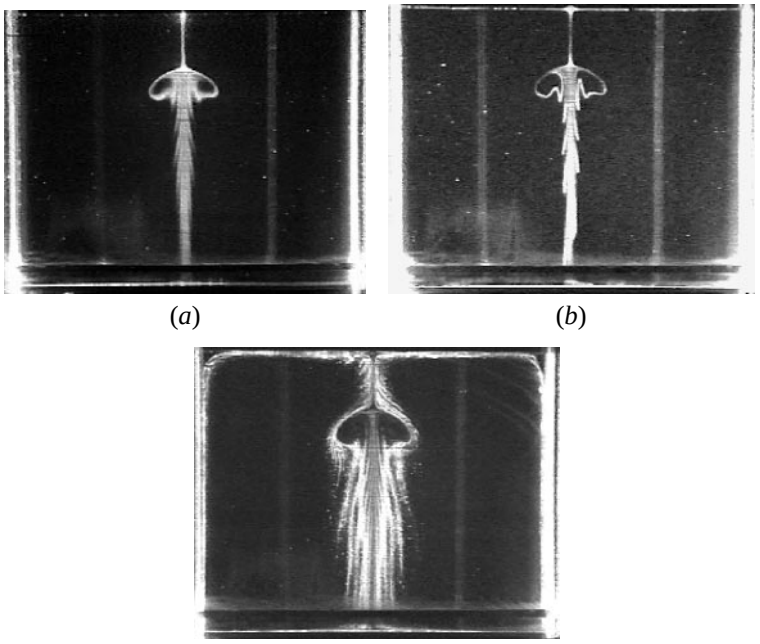

(*a*) (*b*)

(*c*)

FIGURE 4. Vortex breakdown visualized by means of three different techniques for $Re = 1850$ and $H/R = 1.75$ in the rigid cover case. (*a*) The result obtained with the fluorescent dye technique. The dye was injected at the centre of the rigid cover. (*b*,*c*) Corresponding visualizations obtained by electrolytic precipitation. In (*b*) the tracer particles were released from the solder wire at the rigid cover, whereas in (*c*) the marker particles were emitted from the solder wire fixed on the cylinder wall.

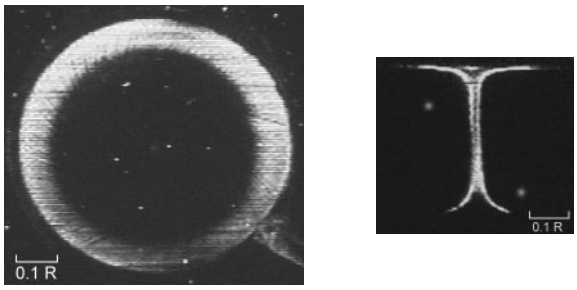

(*a*) (*b*)

FIGURE 5. Emission of tracer particles by electrolytic precipitation of the solder wire at the rigid cover for $Re = 1850$ and $H/R = 1.75$. (*a*) The radial progression in a horizontal plane adjacent to the rigid cover, and (*b*) the progression in a vertical diametral plane.

axisymmetric character of the bubble structure for $H/R = 2$ and $Re = 1852$. Only close to the axis on the rear side of the bubble do asymmetric folds appear.

In order to study the origin of the asymmetry the same tracer distribution as shown in figure 4(*c*) was visualized in several horizontal cross-sections located at different heights z/R above the rotating bottom. The sequence of video frames, figure 7, shows these visualizations in successive planes. Two important observations can be made. First, only in figure 7(*a*), taken just beneath the cover at $z/R = 1.74$ (z is always measured from the rotating bottom), do spirals cross the whole observation plane

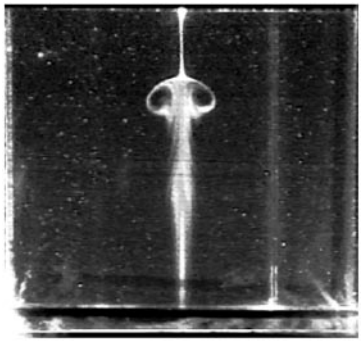

FIGURE 6. Vortex breakdown for $Re = 1852$ and $H/R = 2$ in the rigid cover case. The visualization was obtained with the fluorescent dye technique. The dye was injected at the centre of the rigid cover.

indicating that the radial inflow of tracer particles from the cylinder wall to the central part of the container flow remains restricted to a small region near the cover. Furthermore, the radial inflow does not begin uniformly at the upper circumferencial corner between the cylinder and the cover but, rather, asymmetrically upstream (that is below) of this corner at several discrete locations on the cylinder wall, visible in figure 7(*b*). Second, the video frames 7(*c–h*) illustrate that although each of the streak surfaces caused by these separations is deformed during its motion around the recirculation bubble, its spiral like structure remains clearly visible in the central part of every cross-section. Both of these observations explain why asymmetrically arranged streaks are visible in a vertical diametral plane, as for example in figure 4(*c*). Because of the existence of asymmetric flow separations on the cylinder wall near the rigid cover the streak surface released by the solder wire is split into several parts which cross the central core flow as helicoidal surfaces. In contrast to this, a streak surface released at the rigid cover is not exposed to these separations and, therefore, remains one single continuous surface, as for example in the figures 4(*a*) and 4(*b*).

More details about the flow separations have been obtained by the study of the shear stress direction on the cylinder wall. The powder released by the solder wire is swept along in the direction of the local wall shear stress. Points or lines to which marker particles converge indicate directly the existence of separation points or lines. To examine the powder distribution on the cylinder wall we illuminated a part of this wall by a vertical, 10 mm thick sheet of light, tangent to the inner cylinder wall. Figure 8(*a*,*b*) shows such visualizations for the steady state flow for $H/R = 1.75$ and $Re =$ 1850 and 6000, while the corresponding visualizations of the flow in a vertical diametral plane are presented in figures 8(*c*) and 8(*d*). In figure 8(*a*) for $Re = 1850$ the direction of the wall shear stress remains nearly unchanged over the whole height of the flow domain. In agreement with figure 7 it follows that flow separations can only exist near the cover, where the shear stress is forced to converge since the axial velocity component vanishes. In contrast to this we clearly distinguish at $Re = 6000$ in figure 8(*b*) the convergence of marker particles towards one line situated closer to the rotating disc. Figure 8(*d*) illustrates how the accumulated particles leave the corresponding separation line on the cylinder wall in the radial inward direction. Although the flow regime is unsteady, the position of the separation line remains remarkably stable. If the Reynolds number is further increased the beginning of the separation lines moves closer to the rotating bottom and the radial extent of the separated streak surfaces increases. Similar flow separations are also observed in experiments with a free surface (see Spohn 1991).

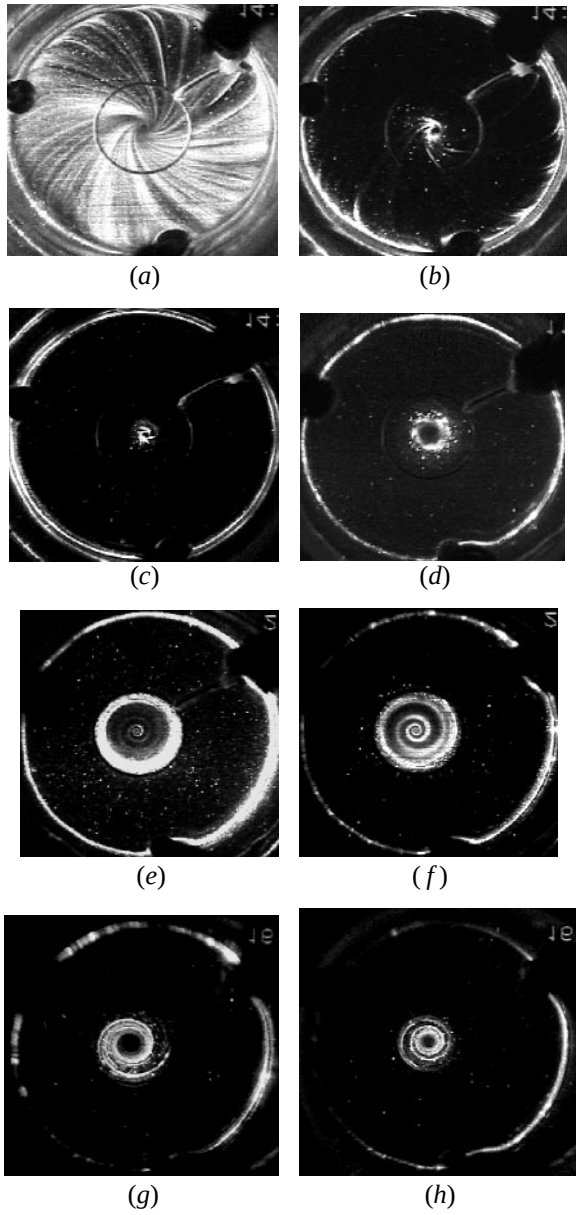

FIGURE 7. Visualization of the flow structure in different horizontal planes with the electrolytic precipitation technique for $Re = 1850$ and $H/R = 1.75$. The tracer particles were released from the solder wire on the cylinder wall. The origin of z is at the rotating bottom. (*a*) $z/R = 1.74$; (*b*) 1.71; (*c*) 1.42; (*d*) 1.40; (*e*) 1.26; (*f*) 1.20; (*g*) 1.09; (*h*) 0.44.

All of these observations indicate that the manifestation of asymmetric separations on the container walls is a fundamental ingredient of container flow. Clearly, the flow in the central part of the container is influenced by the existence of these separations and, as will be seen in the next section, knowledge of these separations is important in analysing the details of the bubble structure and the core flow.

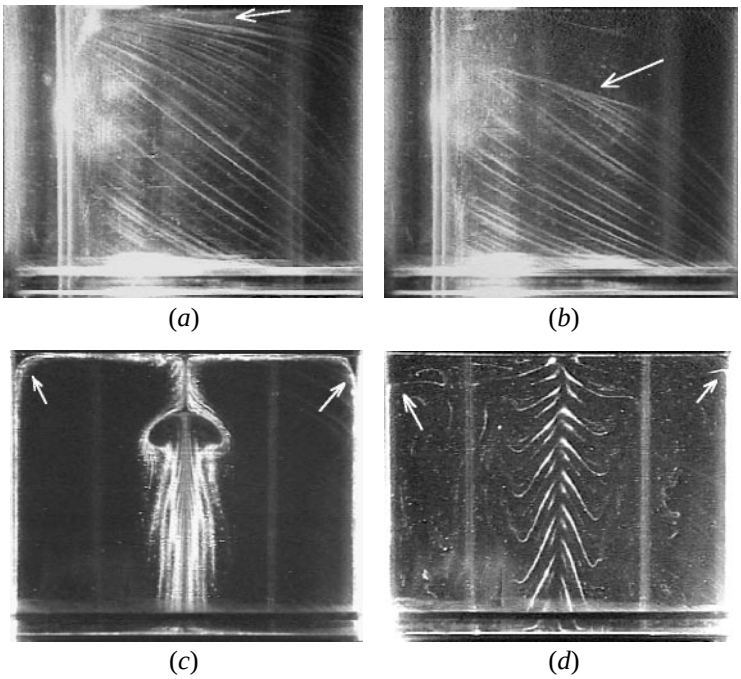

FIGURE 8. Visualization of flow separation by means of the electrolytic precipitation technique in the rigid cover case for $H/R = 1.75$. (*a*, *b*) The wall shear stress direction on the cylinder wall. The arrow marks the position of the separation line. (*c*, *d*) The corresponding flow structure in a diametral plane. (*a*,*c*) $Re = 1850$; (*b*,*d*) $Re = 6000$.

3.2. *Structure of the recirculation bubbles*

In order to study the structure of the recirculation bubbles we observed how the streak surfaces released by the solder wires evolve in time through the central part of the container. The sequence of video frames presented in figure 9 shows this progression in a vertical diametral plane for $H/R = 1.75$ and $Re = 1850$ in the rigid cover case. The tracer particles were released from the solder wire at the rigid cover. To capture more details of the bubble structure the pictures have been enlarged. The non-dimensional times $t^* = \Omega t$ indicated in the figure caption were measured relative to the start-up time of the rotating disc. At about $t^* = 1000$, when according to preliminary observations the steady flow regime was established (see Spohn 1991), the electrolytic precipitation was started. The evolution of the streak surface pattern can be divided into four major sequences. In the first sequence, shown in figure 9(*a*,*b*), the divergence of the streak surface marks the upstream side of the bubble. The visualizations remain highly axisymmetric, illustrating the high degree of symmetry of the upstream side of the bubble. In the second sequence, visible in figure 9(*c*,*d*), asymmetric folds appear successively at the left- and right hand side of the bubble during the radially inward progression of the streak surface along the rear side of the bubble. Each of these folds remains remarkably stable. The third sequence, shown in figure 9(*e*,*f*), illustrates the open character of the bubble. The upper folds of the streak surface move radially inwards and axially upwards into the inner parts of the bubble. At the same time axial stretching and radial compression of the streak surface indicates the existence of opposite axial velocities between the upper and lower folds of the streak surface in combination with decreasing radial inflow. In the fourth sequence, visible in figure

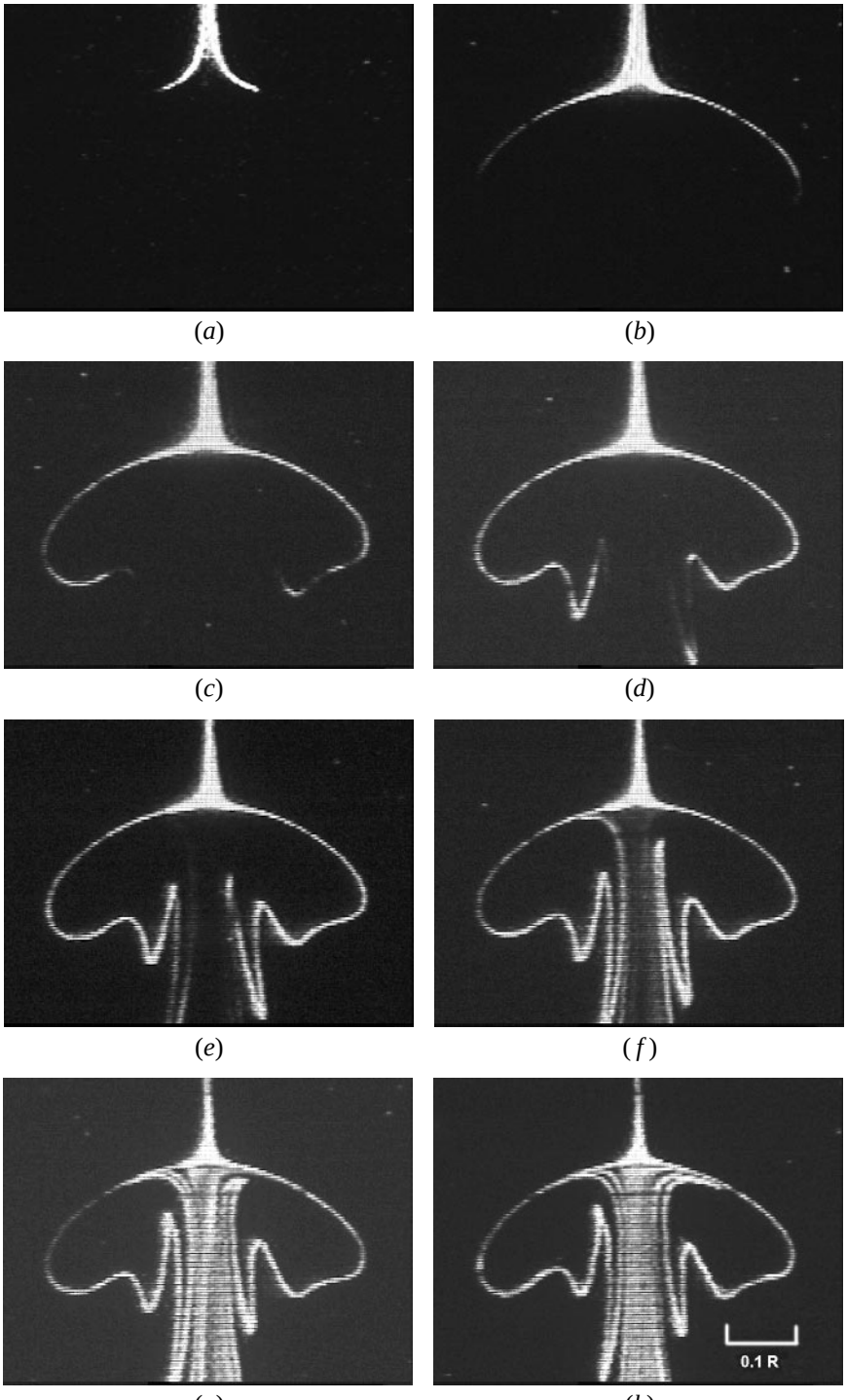

FIGURE 9. Progression in time of the tracer particles around the breakdown bubble for $Re = 1850$, $H/R = 1.75$ in the rigid cover case. The tracer particles were released from the solder wire at the rigid cover. The non-dimensional times $t^* = t\Omega$ are taken relative to the start-up of the rotating bottom. (*a*) $t^* = 1027$; (*b*) 1068; (*c*) 1099; (*d*) 1129; (*e*) 1160; (*f*) 1191; (*g*) 1232; (*h*) 1262.

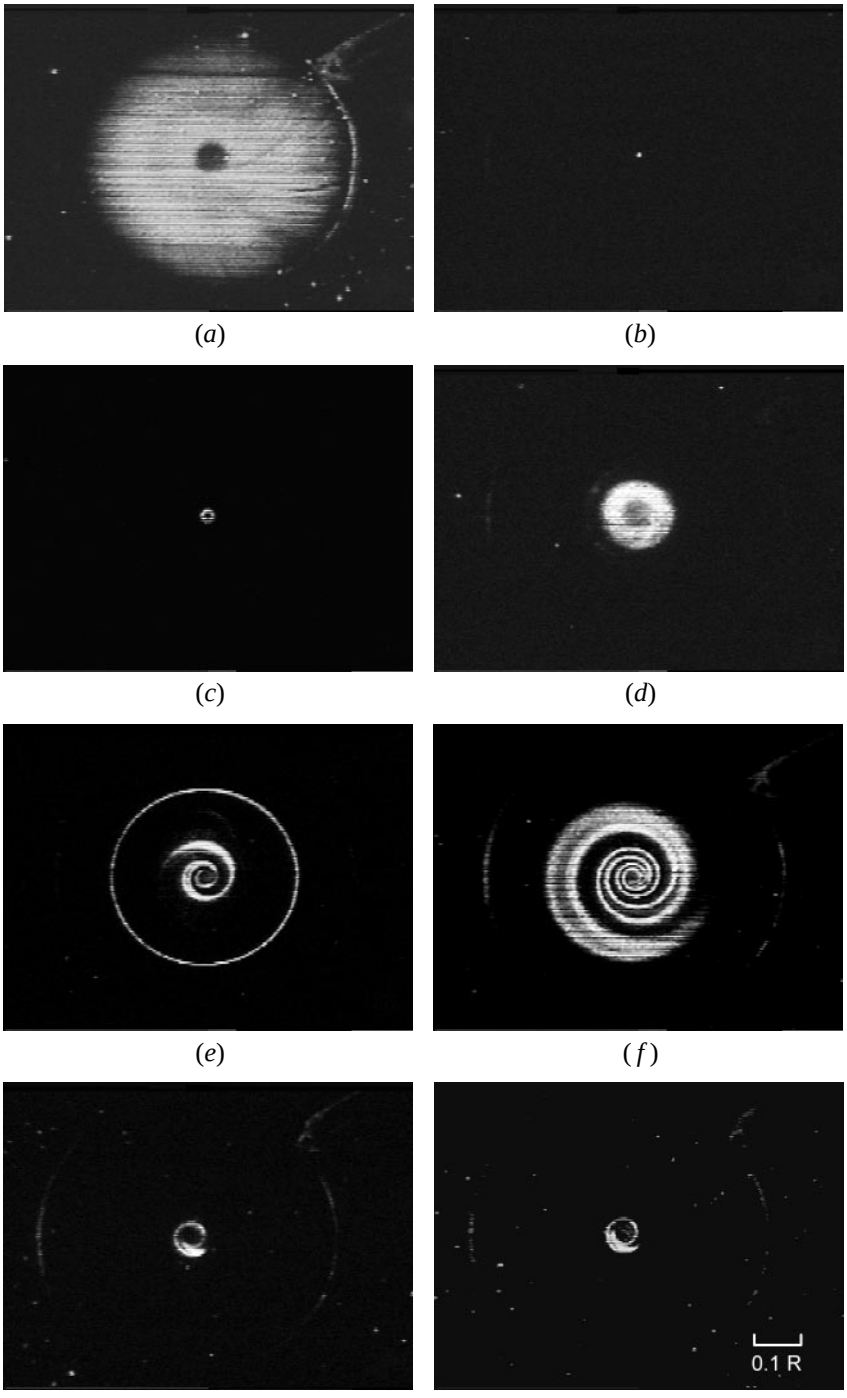

FIGURE 10. Visualization of the flow structure in different horizontal planes with the electrolytic precipitation technique for $Re = 1850$ and $H/R = 1.75$. The tracer particles were released from the solder wire at the rigid cover. (*a*) $z/R = 1.74$; (*b*) 1.71; (*c*) 1.42; (*d*) 1.40; (*e*) 1.26; (*f*) 1.20; (*g*) 1.09; (*h*) 0.44.

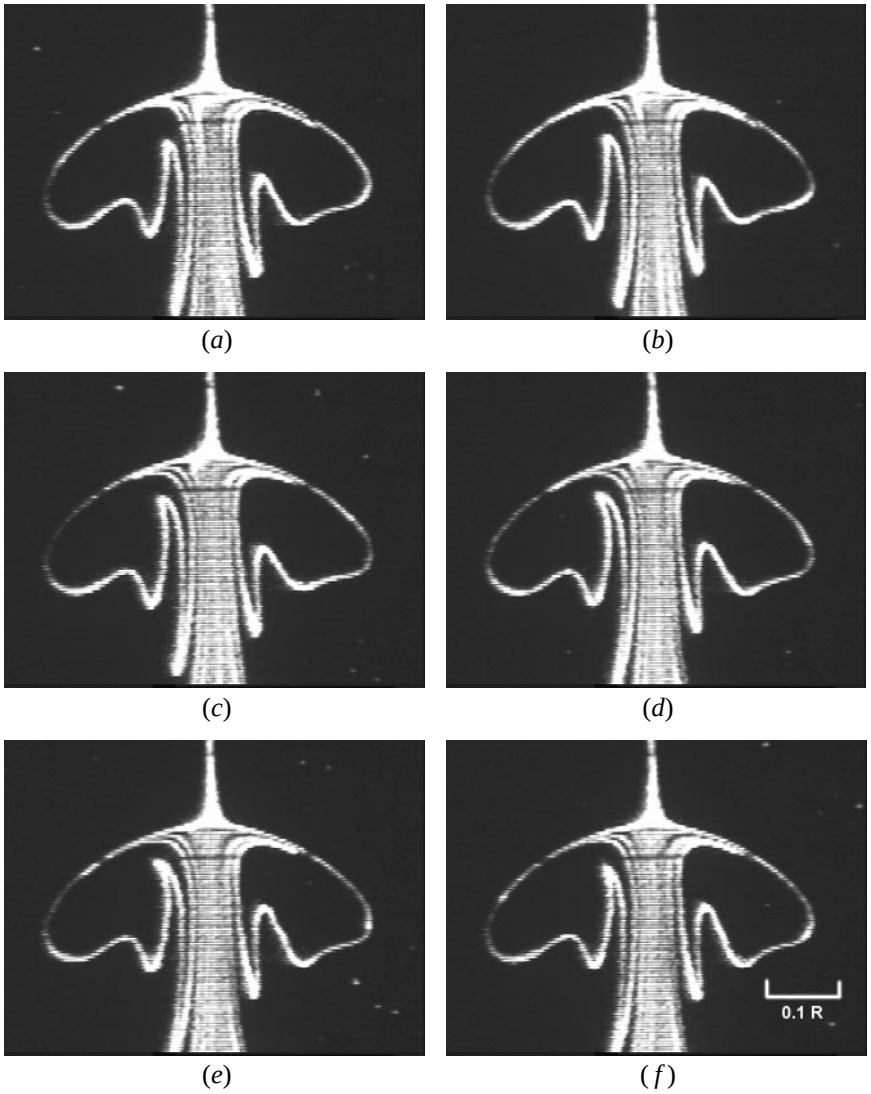

FIGURE 11. Time evolution of the streak surface: the tracer particles were released from the solder wire at the rigid cover for $Re = 1850$, $H/R = 1.75$. (*a*) $t^* = 1242$; (*b*) 1245; (*c*) 1248; (*d*) 1251; (*e*) 1254; (*f*) 1257.

9(*g*,*h*), the tracer particles have nearly stopped their upward progression inside the bubble. The sharp distinction between the downward motion of markers approaching the bubble from its upstream side and the upward motion of the tracer particles inside the bubble clearly implies the existence of a stagnation point which separates both opposite axial motions. Near the container axis the folds of the streak surface are crowded, indicating axial outflow from the bubble interior along the container axis. We notice that during all four sequences two asymmetric oval zones remain clear of markers. Thus, a closed toroidal ring-like region persists inside the bubble, without any visible through flow. The open structure of the bubble is also visible in horizontal cross-sections. Figure 10 shows the evolution of the streak surface pattern in eight successive cross-sections. In figure 10(*d*) the divergence of the streak surface marks the top of the

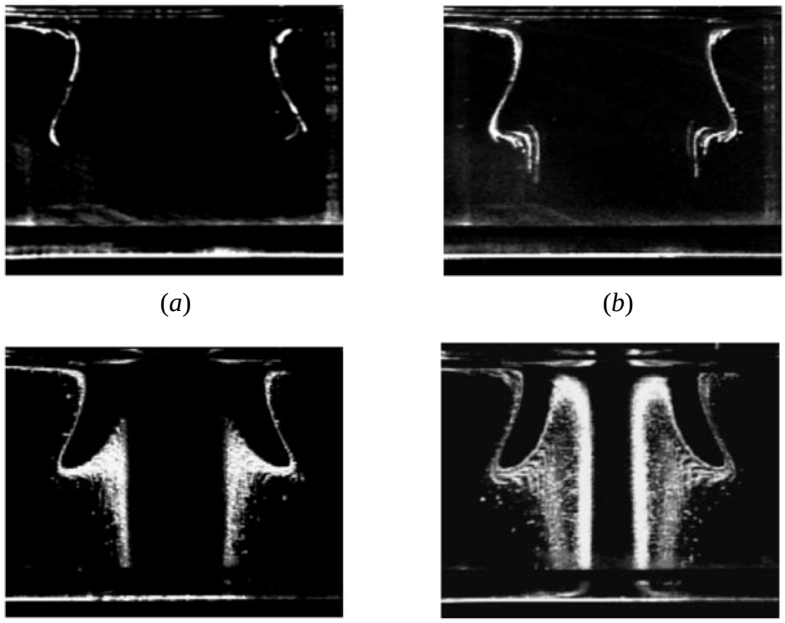

FIGURE 12. Progression in time of the tracer particles around the breakdown region for $Re = 1850$, $H/R = 1.0$ in the free surface case. The tracer particles were released from the solder wire fixed on the cylinder wall. (*a*) $t^* = 3337$; (*b*) 3370; (*c*) 3491; (*d*) 3781.

bubble. Closer to the rear side of the bubble the intersection with the folded streak surface leads to spiral like structures shown in figures 10(*e*) and 10(*f*). The spirals clearly demonstrate that the tracer entered the bubble from its rear side and leaves the bubble interior downwards along the container axis. Finally it should be emphasized that the flow shown in figures 9 and 10 was steady without any visible oscillations of the breakdown bubble. The sequence of video frames presented in figure 11 demonstrates this steady character of the bubble during 2.5 revolution periods of the rotating disc. Each of the successive video frames shows a very similar streak surface pattern without indications of a periodic flow component.

In the free surface case the open structure of the bubbles is also evident. For flow configurations with stationary flow and aspect ratios H/R of about 1 the bubbles are attached to the free surface and show, compared to the rigid cover case, greater radial and axial dimensions (see also Spohn *et al.* 1993). The sequence of video frames presented in figure 12 illustrates the tracer progression in time for the steady flow with $H/R = 1$ and $Re = 1850$. The tracer was released from the solder wire on the cylinder wall. Due to the free surface the mirror images are visible on the top of the figures 12(*c*,*d*). Again, we identify four major sequences. In the first sequence, shown in figure 12(*a*), the streak surfaces just outline the bubble attached to the free surface. In figure 12(*b*), the successive radial inward progression of the streak surface after every half turn marks the lower (downstream) end of the recirculation bubbles. In figure 12(*c*) the backward flow inside the recirculation zone towards the free surface is clearly demonstrated, followed by radial inward flow. Again the tracer particles nearly completely enclose a dark region without any marker, thus illustrating the existence of a toroidal ring without throughflow. Important asymmetric parts of the streak surface, similar to those in figure 9, are not visible. However, inside the recirculation zone near

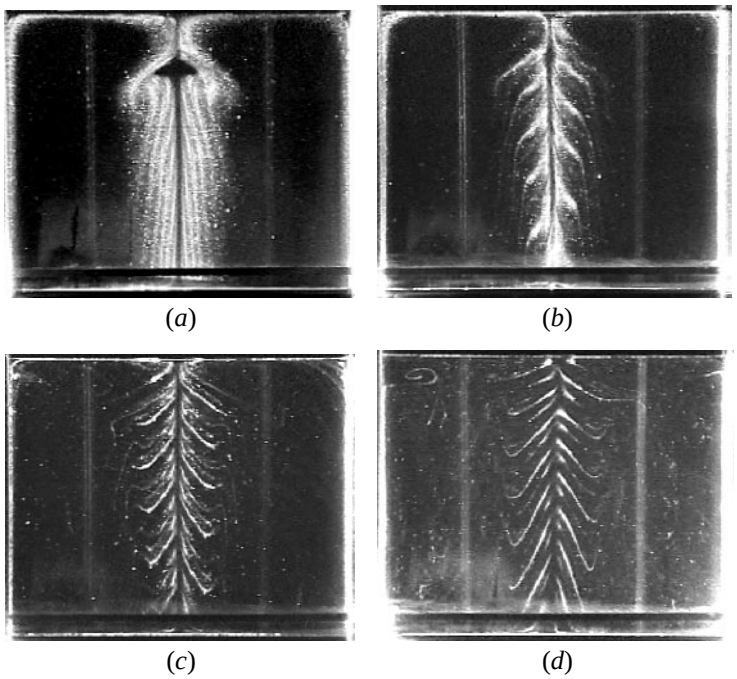

FIGURE 13. Evolution of the steady-state flow with increasing Reynolds number for $H/R = 1.75$ in the rigid cover case. The tracer particles were released from the solder wire fixed on the cylinder wall. (*a*) $Re = 2250$; (*b*) 2750; (*c*) 3500; (*d*) 6000.

the free surface we distinguish in figure 12(*d*) slightly asymmetric boundaries between the concentrated white tracer particles and the uncoloured fluid in the toroidal regions. We suspect that this region corresponds to the region where the folded streak surface is observed in the rigid cover case. The toroidal ring hinders the fluid from advancing radially inwards along the free surface and thus causes the formation of a circular stagnation line at the free surface. It is of interest to point out that although the stagnation point in the rigid cover case is replaced by this circular stagnation line, the bubble structure is similar. Spohn *et al.* (1993) observed that the recirculation bubbles are not always attached to the free surface and the formation of the circular stagnation line is the result of a continuous progression of the bubble position from the interior of the container towards the free surface, as, for a given container aspect ratio, the Reynolds number is increased. The similarity of the bubble structures is, therefore, not surprising.

3.3. *Evolution of the flow structure with increasing Reynolds number*

If the Reynolds number is increased for a given aspect ratio, the evolution of the flow structure is different in the rigid cover and the free surface cases. With a rigid cover the recirculation bubbles disappear above a certain value of the Reynolds number Re which depends on the aspect ratio H/R (see figure 2). In contrast to this, figure 3 shows that the breakdown bubbles in the free surface case are still observed for $Re = 4000$, regardless of the aspect ratio H/R. The observations presented in this subsection illustrate the transformations of the global flow structure which lead to this different evolution of the breakdown bubbles in the parameter space (H/R, Re).

The sequence of video frames presented in figure 13 shows the steady-state flow for $Re = 2250$, 2750, 3500 and 6000 with $H/R = 1.75$ in the rigid cover case. The most

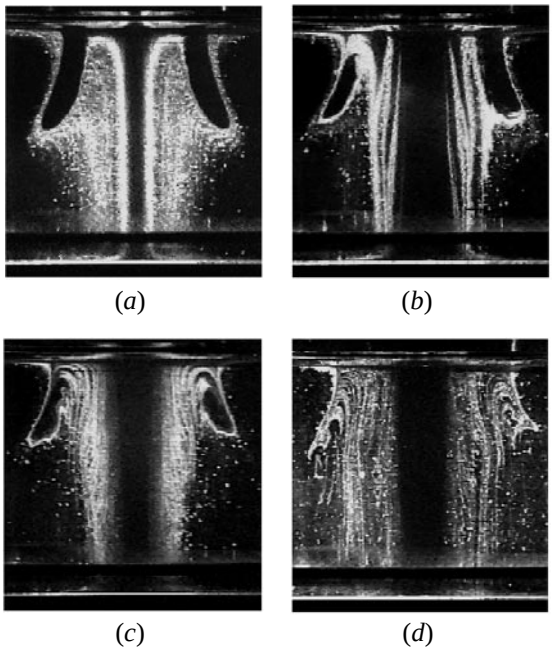

FIGURE 14. Evolution of the steady state flow with increasing Reynolds number for $H/R = 1.0$ in the free surface case. The tracer particles were released from the solder wire fixed on the cylinder wall. (*a*) $Re = 1850$; (*b*) 2350; (*c*) 3000; (*d*) 4000.

important changes of the flow structure appear between $Re = 2250$ (figure 13*a*) and $Re = 2750$ (figure 13*b*). In figure 13(*a*) the breakdown bubble divides the central core into two distinct regions. Upstream of the bubble the streak surfaces are concentrated near the container axis, while downstream of the bubble the same streak surfaces are redistributed over a larger cylindrical region of diameter comparable with the bubble size. In figure 13(*b*) the breakdown bubble has vanished and we see only one, nearly cylindrical core. The helicoidal streak surfaces cross the central part of the container continuously from the rigid cover down to the rotating disc. The streaks are more horizontally oriented around the container axis which indicates a fairly uniform axial velocity. With breakdown bubbles the secondary flow along the container axis undergoes a radial redistribution, while without breakdown bubbles only one cylindrical core with nearly constant axial flow exists along the container axis. When the Reynolds number is further increased to $Re = 6000$ the diameter of the central core increases as shown in figure 13(*d*), but the global flow structure remains nearly unchanged

In the free surface case the disappearance of the breakdown bubbles is less evident. The evolution for $H/R = 1$ at $Re = 1850$, 2500, 3000 and 4000 is shown in figure 14. For all Reynolds numbers a nearly cylindrical core can be distinguished. The diameter of this core, and also the diameter of the torus with the closed recirculation zone, increase with increasing Reynolds number. At the same time the cross-section of the torus decreases. Although in figure 14(*d*) the recirculation zone is still visible it has a more pointed form which makes it difficult to recognize the flow structure inside the bubble. In contrast to the rigid cover case the helicoidal structure of the streak surfaces around the container axis is smeared out. This suggests that in the core region the radial and axial velocities are smaller than in the rigid cover case.

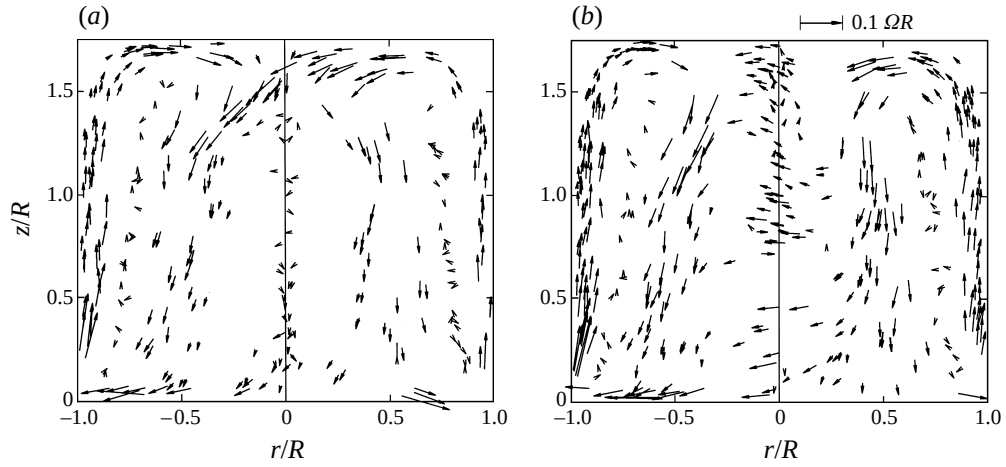

FIGURE 15. Structure of the velocity field in a vertical diametral plane for $H/R = 1.75$ and $Re = 1850$ in (*a*) the rigid cover case, (*b*) the free surface case.

It should be pointed that most of the flows presented in this subsection are unsteady. However, in all cases the structure of the streaks along the cylinder wall remained remarkably stable. In both configurations the axial extent of the central, nearly stationary region grows with increasing Reynolds number. The most important observation is the different evolution of the breakdown bubbles in both configurations which further demonstrates the strong influence of the upper boundary conditions.

3.4. *Structure of the flow around the breakdown bubbles*

In this subsection we present the results of complementary measurements of the velocity field for the two different container configurations, one with a rigid cover and one with a free surface. All measurements were carried out by analysing particle paths as described in §2.2. The velocity field of the secondary flow was measured in a vertical diametral plane, while the azimuthal velocity field was determined in several horizontal sections at different heights above the rotating bottom. Several images obtained with different exposure times have been superimposed to improve the resolution of the measurements in each plane.

Figures 15(*a*) and 15(*b*) show respectively for the rigid cover and the free surface cases the measured velocity field of the secondary flow for $H/R = 1.75$ and $Re = 1850$. For these parameters the steady flow contains in both configurations one breakdown bubble which in figure 15(*a*) is located at some distance beneath the rigid cover (see figure 4) and in figure 15(*b*) is attached to the free surface. Clearly, large radial velocities are restricted to regions near the upper and lower horizontal boundaries of the flow domain. Between these horizontal layers, the flow is confined to two coaxial, nearly cylindrical regions. The outer one, adjacent to the cylinder wall, contains fluid spiralling from the rotating bottom towards the upper boundary, while the inner one channels the flow back from the upper boundary towards the rotating bottom. Both regions are separated by a thin layer with no measurable velocity vectors. The nearly horizontal velocity vectors around the container axis, which are visible in figure 15(*b*), do not represent strong radial velocities but are, rather, caused by the azimuthal motion of particles which remain completely inside the 8 mm thick measurement plane, thus producing misleading paths. The most interesting observation which can be made from figure 15 is that the flow in the vicinity of the breakdown region contains only a

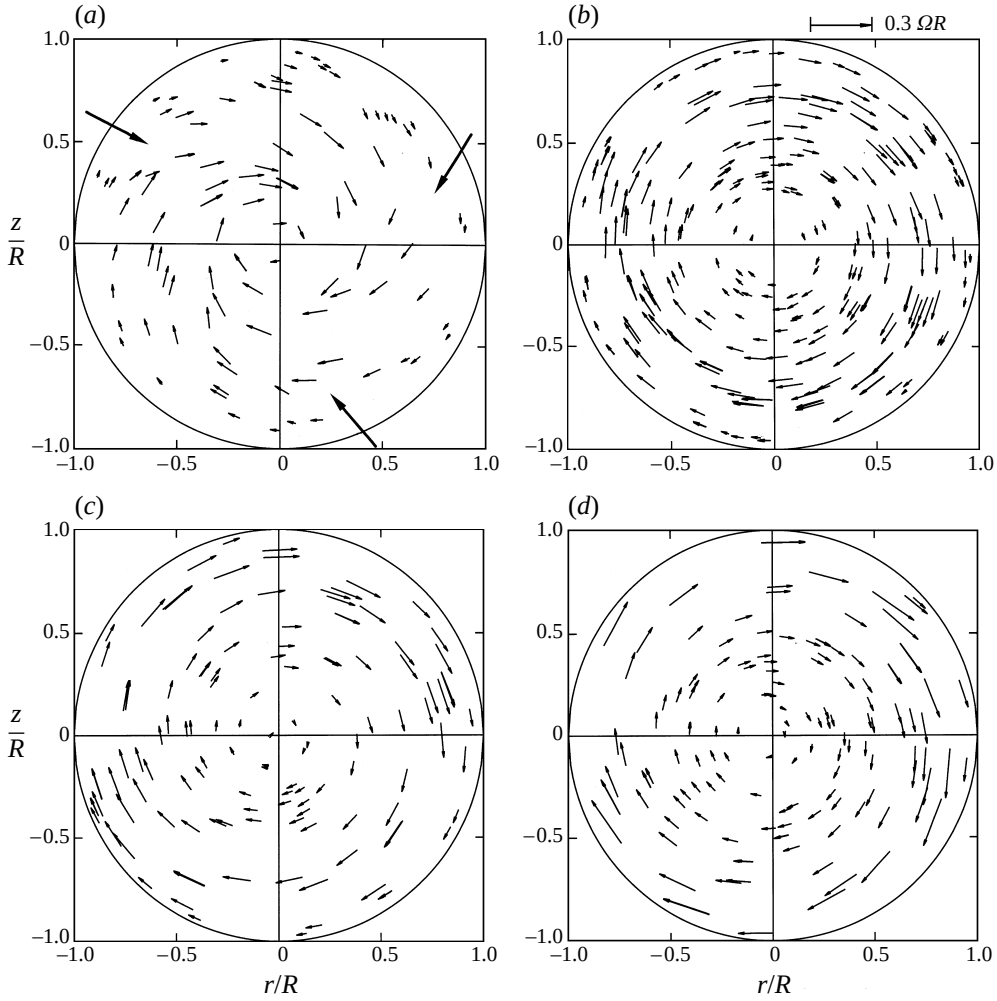

FIGURE 16. Evolution of the velocity field in several successive horizontal planes for $H/R = 1.75$ and $Re = 1850$ in the rigid cover case. The arrows in (*a*) indicate particle-free regions. (*a*) $z/R = 1.64$; (*b*) 1.09; (*c*) 0.73; (*d*) 0.36.

small fraction of the flow rate pumped by the rotating disc. The breakdown bubbles form a part of a nearly cylindrical core inside which the velocities remain small. The axial and radial dimensions of this core depend on the flow parameters (H/R, Re) and the container configuration. It should be emphasized that it is very difficult to analysis particle trajectories in the central region around the core in detail, because in general the number of tracer particles inside the central core is smaller than in the surrounding fluid. The tracer particles used are slightly heavier (by about 2%) than the working fluid and, since inside the core region the small axial velocities cause long residence times of the particles, centrifugation is more efficient.

The azimuthal velocity fields in cross-sections located at different positions z/R above the rotating bottom for $H/R = 1.75$ and $Re = 1850$ in the rigid cover and the free surface cases are shown respectively in figures 16 and 17. Near the upper boundary, at $z/R = 1.64$, (figures 16*a* and 17*a*) regions which are free of particles (marked by arrows) are visible close to the cylinder wall. Since the velocity vectors are

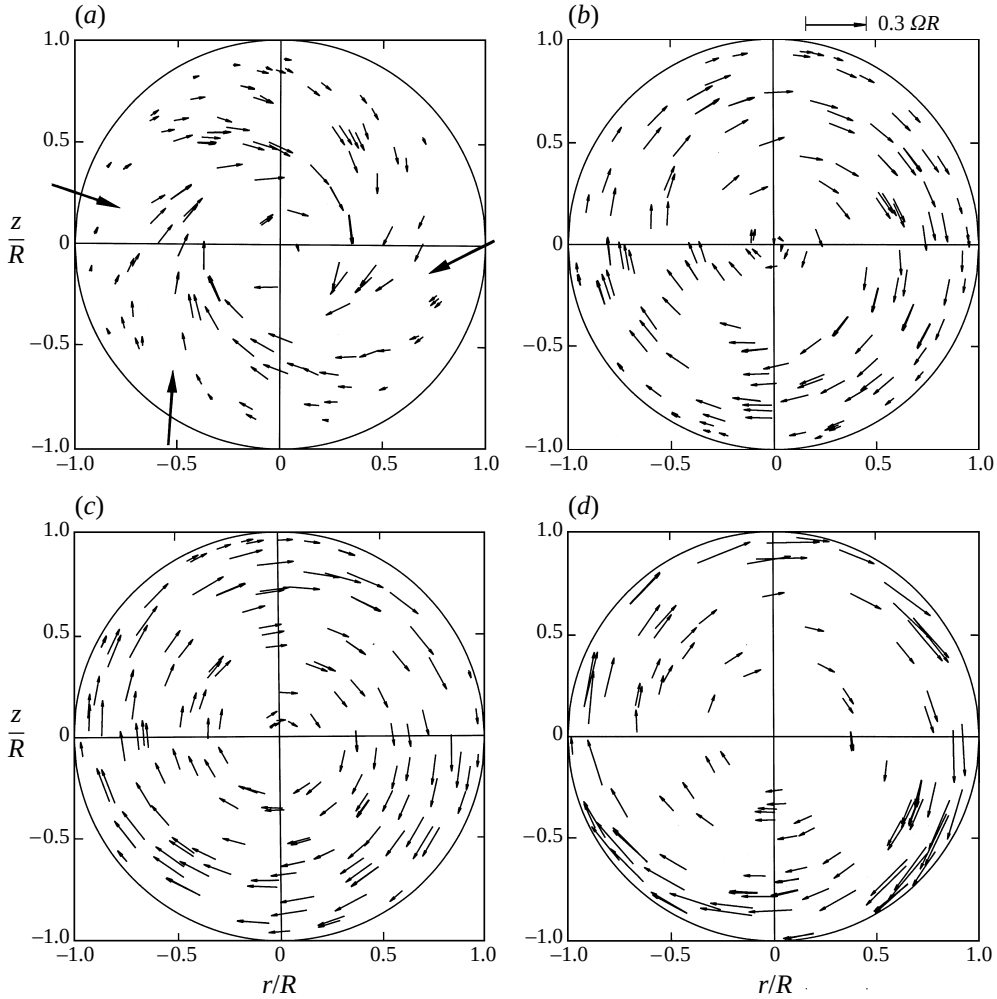

FIGURE 17. Structure of the velocity field in several successive horizontal planes for $H/R = 1.75$ and $Re = 1850$ in the free surface case. The arrows in (*a*) indicate particle-free regions. (*a*) $z/R = 1.64$; (*b*) 1.09; (*c*) 0.73; (*d*) 0.36.

determined from several photographs taken at different times these asymmetries represent systematic features of the flow and are not simply the result of an accidental absence of tracer particles. Comparison with visualizations presented in §3.1 suggests that the particle-free regions are the result of the observed asymmetric flow separations (see figure 7*b*). Further away from the upper boundary and nearer to the middle of the container, a nearly homogenous distribution of the tracer particles is observed in every cross-section (figure 16*b*). Similar to what is observed in trailing vortices, asymmetric aspects of the velocity field are smeared out when progressing along the axis of the vortex flow towards the rotating disc. This does not contradict visualizations presented in §3.1 and §3.2 since the tracer particles used for the velocity measurements represent the instantaneous velocity field, whereas visualizations obtained by means of the electrolytic precipitation technique show the integrated time history of particles emitted from the solder wire fixed on the cylinder wall. The asymmetric aspects of the core flow, in particular on the rear side of the breakdown bubble, could not be captured

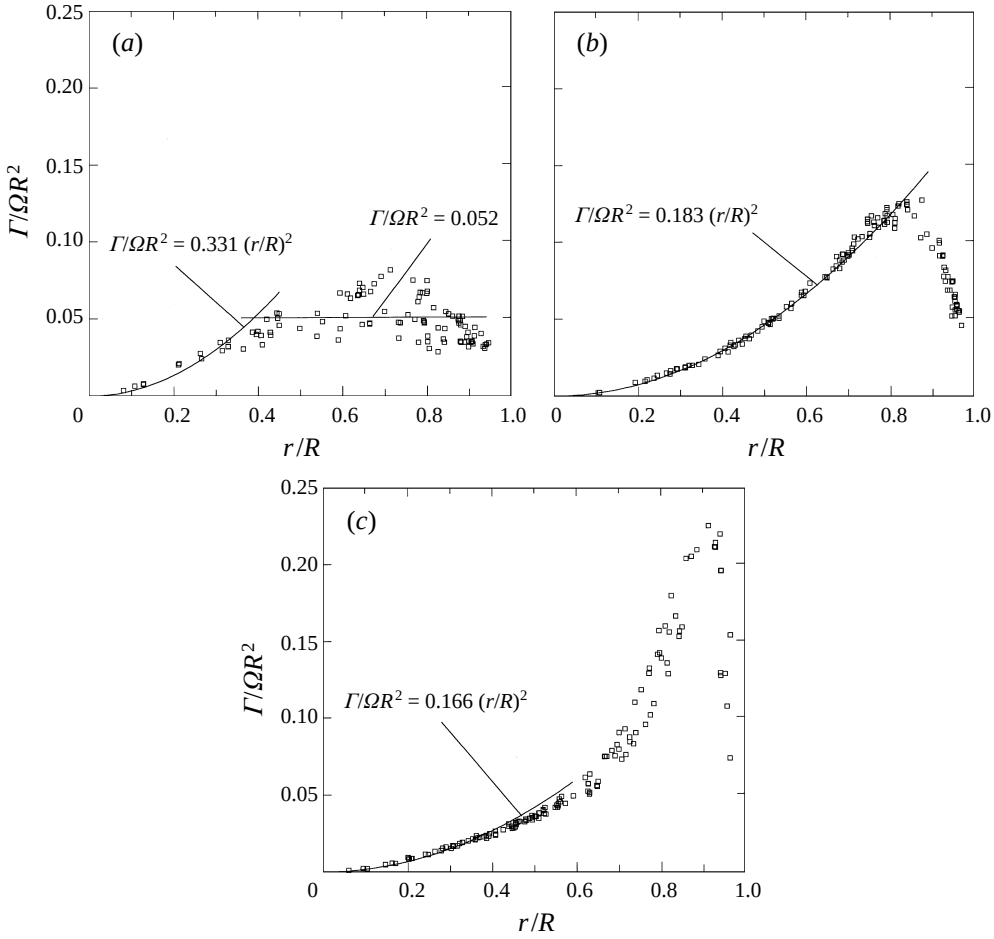

FIGURE 18. Radial distribution of the non-dimensional circulation $\Gamma' = vr/\Omega R^2$ in different horizontal planes for $H/R = 1.75$ and $Re = 1850$ in the rigid cover case. (*a*) $z/R = 1.64$; (*b*) 0.91; (*c*) 0.36.

by our velocity measurements since the number of tracer particles inside this central region was too small.

The influence of the swirl motion on the structure of the vortex flow can be best illustrated by the radial distribution of the circulation $\Gamma(r) = vr$ in different cross-sections. We used the velocity vectors presented in figures 16 and 17 to calculate the radial distribution of the non-dimensional circulation $\Gamma/\Omega R^2$. The results of some selected measurements are shown in figure 18(*a–c*) for the rigid cover case and in figure 19(*a–c*) for the free surface case. In both sequences the axial evolution of the radial profiles attracts particular attention. In figures 18(*a*) and 19(*a*) the circulation near the upper flow domain at $z/R = 1.64$ ($H/R = 1.75$) remains nearly constant between $r/R = 0.4$ and 0.8. We see that the angular momentum is at least partly conserved during the radial inward flow near the upper boundary. The dispersion of the measurements can be explained by the axial gradients of the azimuthal velocity across the 8 mm thick sheet of light. Figure 18(*a*) shows that these gradients are more important near the rigid cover where the no-slip condition influences the flow. Nearer to the rotating disc the radial distribution of the circulation is completely different. In

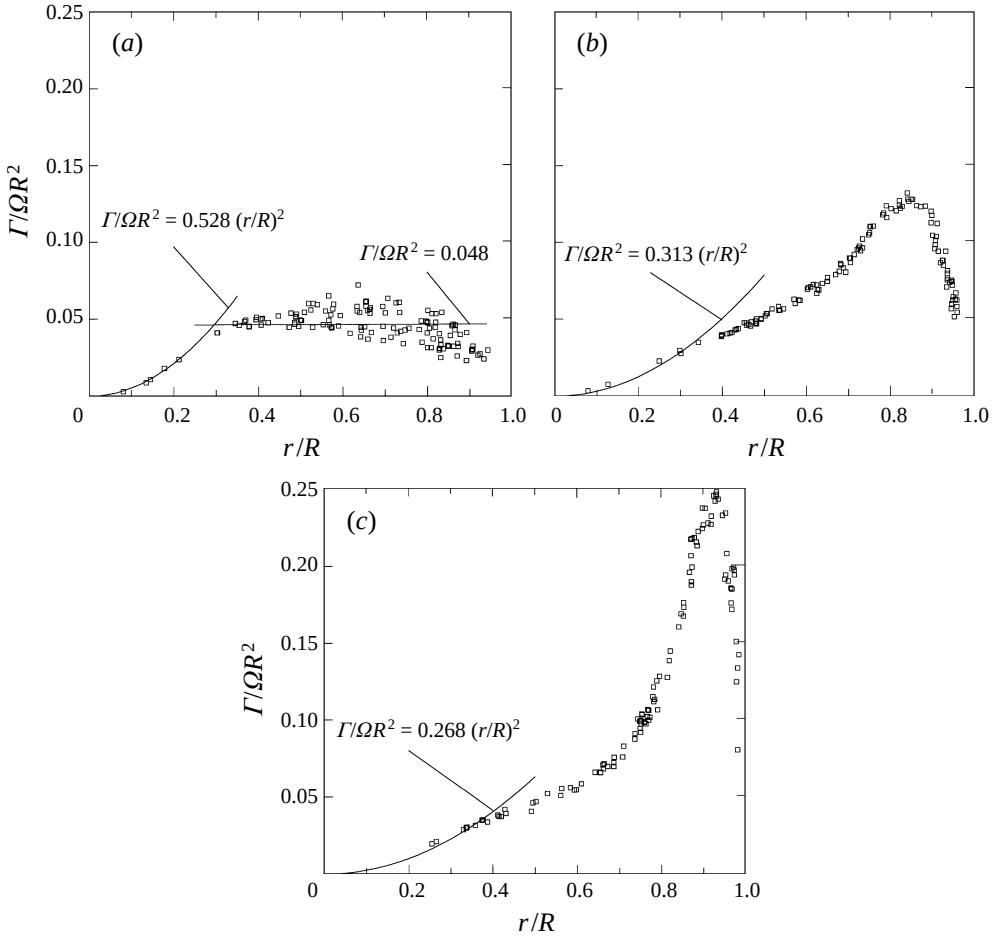

FIGURE 19. Radial distribution of the non-dimensional circulation $\Gamma' = vr/\Omega R^2$ in different horizontal planes for $H/R = 1.75$ and $Re = 1850$ in the free surface case. (*a*) $z/R = 1.64$; (*b*) 0.91; (*c*) 0.36.

figures 18(*b*,*c*) and 19(*b*,*c*) the circulation increases continuously from the container axis towards a maximum located near the container wall and finally decreases rapidly to zero on the cylinder wall. Around the container axis the circulation increases in both configurations as in the case of solid-body rotation. However, in the free surface case the central uniform angular velocity is about 40 % greater than in the rigid cover case. The strength of the circulation varies only slightly in the axial direction for $r/R \leqslant 0.3$, whereas the maximum circulation near the container wall decreases with increasing distance from the rotating bottom. This suggests that along the cylinder wall friction and dissipation decreases the angular momentum of the fluid. Hence, increasing the aspect ratio H/R for a given Reynolds number Re decreases the angular momentum of the fluid arriving near the upper boundary of the flow domain. Therefore, the swirl motion of the container flow is affected by both the aspect ratio H/R and the Reynolds number Re.

4. Conclusions and further discussion

4.1. *Comparison with previous studies of container flows*

We have shown that closed recirculation bubbles are not observed in the present experiments. Instead we find, even in steady flow, open bubbles with permanent in- and outflow. Furthermore, all our visualizations show an asymmetric structure of the streak surfaces which suggests that the flow is not perfectly axisymmetric. Both of these results are surprising in view of previous experimental and numerical studies of container flows and deserve further discussion.

The observed asymmetry has been shown to be real and is not caused by defaults of the visualization techniques. The possible influence of imperfections of the container geometry has also been checked. Imperfections of our installation were so small that even after we changed the angular position of the cylinder or reassembled the installation, we did not find any change in flow structure. Furthermore, as shown in §3.1, the distinctness of the asymmetry depends on the flow parameters (H/R, Re) and configurations with a highly axisymmetric bubble are also observed. The asymmetric structures on the rear side of breakdown bubbles are also visible on photographs presented by Escudier (1984), Böhme *et al.* (1992) and Husain, Hussain & Goldshtik (1995). In our experiments this asymmetry is more clearly identified because the electrolytic precipitation method, used in the present study, gives a better resolution of the structure. This explains why flow regions with closely folded streak surfaces, as for example on the rear side of the recirculation zones close to the container axis, appear almost uniformly coloured with the fluorescent dye technique, whereas individual folds of the streak surface are visible with the electrolytic precipitation method. Our observations are, therefore, not contradictory to previous studies, especially those of Escudier (1984), but show details of the flow structure which were not captured with other visualization techniques.

The observed flow separations at the upper corner between the rigid cover and the cylinder wall, which are the principal cause for the asymmetry, cannot be explained by the onset of centrifugal instabilities similar to the appearance of Görtler vortices. The velocity profiles presented in figures 18 and 19 remain stable along the cylinder wall according to the Görtler criterion. The boundary layer beneath the cover also seems stable. The radial distribution of the circulation indicates that the Reynolds number of this boundary layer is about 0.06 times the Reynolds number of the rotating disc. This value remains well below 625 for which Savas (1987) observed the onset of instability of such a boundary layer. The boundary layer above the rotating disc becomes unstable for Reynolds numbers of $O(10^4)$ which is well above the range considered here. Nevertheless, the experiments indicate that the flow must be sensitive to asymmetric perturbations. It should be emphasized that although recent numerical simulations of Gelfgat, Bar-yoseph & Solan (1996) demonstrate the stability of the container flow with respect to axisymmetric perturbations, the influence of asymmetric perturbations is not yet well understood.

The new insight into some particular aspects of container flow allows also a more detailed comparison with predictions of numerical simulations. Previous numerical studies by Lugt & Abboud (1987), Neitzel (1988), Lopez (1990), among others, noted an excellent agreement between their calculated bubble position and the visualizations presented by Escudier (1984). However, details of the breakdown bubble, as observed in the present study, are not correctly predicted by these simulations. For steady flow in all cases the calculated structure of the recirculation zone is closed and by assumption axisymmetric, in contrast to the in- and outflow and the asymmetry found

in our experiments. The demonstration of these asymmetries is particularly important if we reconsider some recent arguments of Lopez & Perry (1992) to explain the formation of streaks on the rear side of the recirculation bubbles. Lopez & Perry assumed an axisymmetric container flow with injection of dye at the centre of the rigid cover and explained the formation of streaks on the rear side of the recirculation bubbles by axial oscillations of the central core flow which cause periodic in- and outflow. According to the observations presented in §3.1 and §3.3 similar streaks exist in steady flow also and are caused by asymmetric flow separations on the container walls. In this case the folded structure of the streak surface on the rear side of the recirculation zone was not due to periodic oscillations of the bubble. Instead the visualizations, presented in §3.1, show that on the rear side of the bubble the streak surfaces caused by the flow separations on the container wall fit into the folds of the streak surface released by the solder wire at the rigid cover. At the same time the amplitude of the folds increases towards the container axis. This suggests that the radially converging and axially diverging flow in this region amplifies asymmetries caused by the separations on the container wall. Finally it should be mentioned that although this discussion is devoted to the observation of streaks in steady flow we also observed that in configurations with unsteady flow, axial oscillations of the recirculation bubbles add a periodic component to the otherwise constant radial inflow between the rear side of the bubble and the rotating bottom and thus contribute to the wrinkled structure of the streak surfaces.

4.2. *Vortex breakdown*

The value of closed container flows for studies of vortex breakdown seems not to be generally accepted. While Escudier (1984) identified the bubbles inside container flow as vortex breakdown, Ronnenberg (1977) and Leibovich (1984) classified them as simple recirculation phenomena. The observations presented in §3 show some further characteristics which underline the similarity of breakdown bubbles in container flow with breakdown bubbles observed in vortex tubes. According to Hall (1972) breakdown bubbles are distinguished by three different characteristics: a free stagnation point in combination with reversed axial flow, the divergence of the stream tubes upstream of the bubble and finally the existence of an adverse pressure gradient along the rotation axis. The visualizations in the rigid cover configuration, presented in §3.2, clearly show the existence of a free stagnation point in combination with reversed axial flow. In addition, the velocity measurements presented in §3.4 show that the bubbles are always imbedded inside an axial flow, which is directed from the rigid cover towards the rotating bottom. Hence, viscous forces tend to drag the fluid along the container axis and hinder the formation of an on-axis stagnation point. Consequently, adverse axial pressure gradients must exist along the container axis to explain the formation of the observed on-axis stagnation points. Now, the structure of the secondary flow, presented in §3.4, indicates two possible origins for such axial pressure gradients. First, the thickness of the boundary layer along the cylinder wall grows with increasing distance from the rotating bottom. Thus, the effect of this boundary layer on the axial flow along the container axis is similar to the effect of a diverging tube which imposes an adverse pressure gradient along its axis. Second, along both container extremities the radial distribution of the axial in- and outflow of the core region is different. Near the rigid cover the axial inflow is concentrated closer to the container axis, while above the rotating disc the axial outflow takes place over nearly the whole diameter of the container. The resulting deficit of the axial flow rate between these two regions must be compensated inside the core region. An adverse axial pressure gradient must cause

radial outwards flow inside the core. The relative importance of each of these mechanisms depends on H/R and Re, and is difficult to determine from our qualitative observations. The similarity of breakdown bubbles in the container and vortex tubes is further supported by our observations of the bubble structure itself. In particular we found, as in the experiments of Leibovich (1978), that the bubble remains highly axisymmetric on its upstream side while its downstream side appears asymmetric. More important is the fact that the breakdown bubbles inside the container flow are open. All experimental observations of vortex breakdown that we are aware of show such an open structure of the bubble with in- and outflow.

Particularly interesting in the context of previous observations of vortex breakdown are the experiments with bubbles attached to the free surface. These differ in two main points from the description of vortex breakdown given by Hall. First, the stagnation point changes into a stagnation line and second, no adverse axial pressure gradient and no divergence of the stream tubes exist upstream of the bubble in the axial direction. However, previous experiments (Spohn *et al.* 1993) showed that these attached bubbles are the result of a continuous progression of the bubble position from the interior of the flow domain towards the free surface as Re is increased for given H/R. During this progression no change in the physical mechanism can be observed. This suggests that the attached recirculation bubbles can also be considered as breakdown phenomena.

Although we classify the recirculation zones inside container flow as breakdown bubbles, some of their characteristics differ from previous observations made in other arrangements. Leibovich (1984), for example, described the breakdown wake inside a vortex tube as invariably turbulent with strong coherent oscillations, whereas the visualizations presented in §3.2 show a laminar and stationary breakdown wake. In addition, previous studies reported that the breakdown bubbles themselves oscillate. Faler & Leibovich (1977) observed symmetric, axial oscillations of the bubble, and Brücker & Althaus (1992) found asymmetric bubble oscillations. Both studies attribute the in- and outflow of the breakdown bubbles to these periodic symmetric or asymmetric oscillations and conclude that unsteadiness is a fundamental ingredient of vortex breakdown. However, in §3.2 we showed that open breakdown bubbles may also exist in stationary flow. The open structure of the bubble was not due to any detectable periodic bubble motions. Hence, in general, it seems not justified to assume unsteadiness of the phenomenon as a basic ingredient. However, it should be emphasized that we also observed unsteady breakdown bubbles. In such cases we noted either asymmetric or axisymmetric oscillations of the bubbles in agreement with previous findings.

The velocity measurements presented in §3.4 give some additional information on the particular characteristics of the vortex flow inside the container. In the general case of a confined rotating flow Lewellen (1962) showed that these characteristics are described by three non-dimensional parameters: the axial Reynolds number $Re_Q = Q/L\nu$, the swirl parameter $S = 2\pi\Gamma a/Q$ and the aspect ratio L/a, where Q is the flow rate along the rotation axis, Γ the maximum circulation and L and a are respectively the characteristic length and radius of the rotating flow. In the case of the container flow the central core region occupies nearly the whole flow domain so that $L \approx H$ and $a \approx R$. Hence, the axial flow rate is $Q \approx \pi R^2 w$ and the maximum circulation $\Gamma \approx vR$, where w represents the characteristic axial velocity and v the characteristic azimuthal velocity. For the flow configurations considered here, we find with the help of the velocity measurements presented in §3.4 that $S \approx 10$ and $Re_Q \approx 100$. Table 1 compares these values with the corresponding values of other confined flows with vortex breakdown. Clearly, container flow can be distinguished by its greater swirl parameter.

Authors	Arrangement	S	Re_Q
Faler & Leibovich (1977)	Vortex tube with radial inlet guidevanes	0.4–0.7	75–150
Escudier (1988)	Vortex tube with radial inlet guidevanes	0.5	200
Brücker & Althaus (1992)	Vortex tube with axial inlet guidevanes	0.6	Length of tube unknown
Present study	Closed cylindrical container with rotating bottom	10	100

TABLE 1. Comparison of the Reynolds number $Re_Q = Q/(\nu H)$ and the swirl parameter $S = 2\pi\Gamma R/Q$ in confined vortex flows with vortex breakdown. H is the length of the vortex axis, R the radius of the vortex, Γ the maximum circulation in the vortex, ν the kinematic viscosity of the fluid and Q the axial volume flow rate.

In principal it is, therefore, not surprising that some of the breakdown characteristics are different. But these differences help to distinguish between characteristics inherent to the phenomenon, visible whenever the phenomenon appears, and characteristics which are secondary.

Parts of this work were financially supported by the contract DRET No. 89.130. The first author is grateful for a grant of the CEE Science Programme. We especially want to express our gratitude to S. Layat and Barbier-Neyret from the Laboratoire des Ecoulements Géophysiques et Industriels et P. Lacombe from the Laboratoire d'Etudes Aérodynamiques for their technical assistance.

REFERENCES

BÖHME, G., RUBART, L. & STENGER, M. 1992 Vortex breakdown in shear-thinning liquid: experiment and numerical simulation. *J. Non-Newtonian Fluid Mech.* **45**, 1–19.

BRÜCKER, C. & ALTHAUS, W. 1992 Study of vortex breakdown by particle tracking velocimetry (PTV). Part 1: Bubble type vortex breakdown. *Exps. Fluids* **13**, 339–349.

DAVIS, J. T. & RIDEAL, E. K. 1963 *Interfacial Phenomena.* Academic.

ESCUDIER, M. P. 1984 Observations of the flow produced in a cylindrical container by a rotating end wall. *Exps. Fluids* **2**, 179–186.

ESCUDIER, M. P. 1988 Vortex breakdown: Observations and explanations. *Prog. Aerospace Sci.* **25**, 179–229.

FALER, J. H. & LEIBOVICH, S. 1977 Disrupted states of vortex breakdown. *Phys. Fluids* **19**, 1285–1300.

FALER, J. H. & LEIBOVICH, S. 1978 An experimental map of the internal structure of vortex breakdown. *J. Fluid Mech.* **86**, 312–337.

GELFGAT, A.YU. BAR-YOSEPH P. Z. & SOLAN A. 1996 Stability of confined swirling flow with and without vortex breakdown. *J. Fluid Mech.* **311**, 1–36.

GRANGER, R. A. 1990 The breakdown of a vortex. *Appl. Mech. Rev.* **43**, 151.

HALL, M. G. 1967 A new approach to vortex breakdown. *Proc. Heat Transfer Fluid Mech. Inst.*, pp. 318–340. Univ. California, San Diego, La Jolla, Cal., USA.

HALL, M. G. 1972 Vortex breakdown. *Ann. Rev. Fluid Mech.* **4**, 185–217.

HARVEY, J. K. 1962 Some observations of the vortex breakdown phenomenon. *J. Fluid Mech.* **13**, 585–593.7

HONJI, H., TANEDA, S. & TATSUNO, M. 1980 Some practical details of the electrolytic precipitation method of flow visualisation. *Rep. Res. Inst. of Appl. Mech.*, XXVIII. Kyushu University, Fukuoka, Japan.

Husain, H. S., Hussain, F. & Goldshtik, M. 1995 Anomalous separation of homogeneous particle-fluid mixtures: Further observations. *Phys. Rev.* E, **52**, 4909–4923.

Krause, E. & Liu, C. H. 1989 Numerical studies of incompressible flow around delta and double-delta wings. *Z. Flugwiss. Weltraumforsch.* **13**, 291–301.

Leibovich, S. 1978 Vortex breakdown. *Ann. Rev. Fluid Mech.* **4**, 185–217.

Leibovich, S. 1984 Vortex stability and breakdown: survey and extension. *AIAA J.* **22**, 1182–1196.

Lewellen, W. S. 1962 A solution for three-dimensional vortex flows with strong circulation. *J. Fluid Mech.* **13**, 419–432.

Lopez, J. M. 1990 Axisymmetric vortex breakdown Part 1. Confined swirling flow. *J. Fluid Mech.* **221**, 533–552.

Lopez, J. M. & Perry, A. D. 1992 Axisymmetric vortex breakdown. Part 3 Onset of periodic flow and chaotic advection. *J. Fluid Mech.* **234**, 449–471.

Lugt, H. J. 1989 Vortex breakdown in atmospheric columnar vortices. *Bull. Am. Met. Soc.* **70**, 1426–1437.

Lugt, H. J. & Abboud, M. 1987 Axisymmetric vortex breakdown in a container with a rotating lid. *J. Fluid Mech.* **179**, 179–190.

Lugt, H. J. & Haussling, H. J. 1982 Axisymmetric vortex breakdown in rotating fluid within a container. *Trans. ASME* I: *J. Appl. Mech.* **49**, 921–922.

Menne, S. & Liu, C. H. 1990 Numerical simulation of a three-dimensional vortex breakdown. *Z. Flugwiss. Weltraumforsch.* **14**, 301–308.

Neitzel, G. P. 1988 Streak-line motion during steady and unsteady axisymmetric vortex breakdown. *Phys. Fluids* **41**, 958–960.

Ronnenberg, B. 1977 Ein selbstjustierendes 3-Komponenten-Laserdoppleranemometer nach dem Vergleichsverfahren, angewandt auf Untersuchungen in einer stationären zylinder- symmetrischen Drehströmung mit einem Rückströmgebiet. *Max-Planck-Institut für Strömungsforschung, Göttingen*, Bericht 19.

Sarpkaya, T. 1971 On stationary and travelling vortex breakdowns. *J. Fluid Mech.* **45**, 545–559.

Savas, Ö. 1987 Stability of Bödewardt flow. *J. Fluid Mech.* **183**, 77–94.

Spall, R. E., Gatski, T. B. & Ash, R. L. 1990 The structure and dynamics of bubble-type vortex breakdown. *Proc. R. Soc. Lond.* A **429**, 612–637.

Spohn, A. 1991 Ecoulement et éclatement tourbillonnaires engendrés par un disque tournant dans une enceinte cylindrique. PhD thesis, Université Joseph Fourier-Grenoble.

Spohn, A., Mory, M. & Hopfinger, E. J. 1993 Observations of vortex breakdown in an open cylindrical container with rotating bottom. *Exps. Fluids* **13**, 70–77.

Vogel, H. U. 1968 Experimentelle Ergebnisse über die laminare Strömung in einem zylindrischen Gehäuse mit darin rotierender Scheibe. *Max-Planck-Institut für Strömungsforschung, Göttingen, Bericht* 6.

Vogel, H. U. 1975 Rückströmblasen in Drallströmungen. *Festschrift 50 Jahre Max-Planck-Inst. für Strömungsforschung, Hubert Göttingen*, pp. 263–272.